Colloid Polym Sci 277:743–751 (1999)

ORIGINAL CONTRIBUTION

M.A. Valdez
O. Manero

Rheology of dilute polyelectrolyte solutions in narrow channels

Received: 26 September 1998
Accepted in revised form: 11 March 1999

M.A. Valdez (✉)
Departamento de Física
Universidad de Sonora
Ap. postal 1626
83000 Hermosillo Son.
Mexico
e-mail: valdez@eudeve.fisica.uson.mx

O. Manero
Instiuto de Investigación en Materiales
UNAM, Ap. postal 70-360
04510 Mexico D. F.
Mexico

Abstract The shear flow of dilute polyelectrolyte solutions bounded by either neutral or repulsive walls is modeled using a nonlinear dumbbell with conformation-dependent friction. Assuming that the configurational probability density function depends on the internal coordinates (**r**) and the distance of the center of mass of the molecule to the walls, coupled differential equations for the tensor moments $\langle \mathbf{rr} \rangle$ are obtained. Coulombic repulsion between beads is considered to simulate the charge repulsion between ionized sites distributed along the backbone of a real polyelectrolyte. The repulsive interaction between the polyelectrolyte molecule and the charged walls is that of the DLVO model and the molecule is considered to be a charged sphere. Numerical solutions for the components of the tensor $\langle \mathbf{rr} \rangle$ are worked out with the preaverage approach, and only when neutral walls considered are exact solutions obtained. Viscosity results show that in the limit of very wide channels, the corresponding viscosity in the bulk is obtained. The wall repulsion on the charged molecules produces migration of molecules towards the center of the channel resulting in a depleted layer with lower viscosity next to the walls. The calculated slip phenomenon using the method employed by Grisafi and Brunn is dependent on the beads repulsion and the shear rate. The slip velocity obtained with the Mooney method shows similarities with available experimental results for polyelectrolyte solutions. Birefringence calculations are performed in narrow and wide channels for different bead repulsions, with interesting results for both flexible and rigid molecules.

Key words Nonlinear dumbbell model · Polyelectrolyte solutions · Narrow channels · Flow birefringence · Slip velocity

Introduction

Macromolecules in dilute polymer solutions have usually been modeled as Hookean dumbbells and this simple model enables the prediction of various rheological properties. Most of these predictions consider an unbounded domain and no interactions between dumbbells. However, relatively less attention has been paid to the prediction of rheological properties in confined geometries [1–3] where distinct phenomena occur, as for example, the existence of an apparent slip close to the domain solid boundaries.

Inclusion of hydrodynamic interactions in the dumbbell formulation leads to the prediction of interesting features, such as the drag being anisotropic in space. The result is a transversal migration effect which depends on the size of the dumbbell beads [4]. It is known that the Hookean spring model cannot predict the reduction in the shear viscosity with shear rate [1] and nonlinear models have been proposed, some of them with additional features, such as a Warner connector and conformation – dependent hydrodynamic friction [5], first suggested by de Gennes [6]. Simulations performed for dilute polymer solutions show that the use of a

conformation – dependent friction coefficient is a more realistic approach in some circumstances to predict the birefringence behavior observed in dilute polyelectrolyte solutions [7].

It is well known that the molecular conformation of polyelectrolytes in dilute solutions is greatly influenced by the ionic strength of the solvent. When this is low, a highly extended conformation of the polyelectrolyte gives rise to rheological behavior similar to that observed in rigid rods. On the other hand, as the ionic strength increases, the behavior in flow resembles that of a flexible macromolecule with a coiled equilibrium conformation.

Simulations of the flow of polyelectrolyte solutions in unbounded media have been performed considering a dumbbell with charged beads and a nonlinear connector joining them. The predicted rheological behavior and comparisons with experimental data in a general two-dimensional flow have been widely treated by Dunlap and Leal [8]. As observed in the experiments, the simulated behavior when the repulsion between charges is varied reproduces that of a flexible molecule (low repulsion) and that of a rigid rod (high repulsion); however, interactions with solid boundaries have not been considered in these models so far, and no attention has been given to polyelectrolyte solutions flowing in confined geometries. It is known that the flow of nonionic macromolecules in confined media gives rise to interesting phenomena, and these phenomena are highly dependent on the molecular conformation: rigid or flexible macromolecules behave differently in confined geometries.

It is the aim of the present work to simulate the rheological behavior of dilute polyelectrolyte solutions in shear flow between parallel walls. Attention is given to the drastically different rheological behavior exhibited when the repulsion of charges is modified. Polyelectrolytes are represented by a nonlinear dumbbell model which includes conformation-dependent friction. Coulombic repulsion between beads is considered to simulate charge repulsion between the ionized groups of the chain. As explained by Dunlap and Leal [8], each bead is assigned an effective charge to obtain a desired degree of chain expansion. In the first stage, the walls are assumed to be rigid and neutral. Secondly, the electrostatic repulsion between the charged walls and the charged macromolecules is considered. To a first approximation, this repulsion is modeled as that existing between two infinite charged walls and a spherical charge [9]. This is obviously a rough approximation, but this approach is the simplest one necessary to facilitate an understanding of the rheological behavior of polyelectrolytes in confined media.

With the use of the preaverage approximation, we obtain a coupled differential equation system for the moments of the tensor $\langle \mathbf{rr} \rangle$ in stationary conditions, and from these the moments, stress tensor, viscosity and birefringence can be calculated straightforwardly. Results for the viscosity of the solution are dependent on the size of the channel and the wall repulsion and for sufficiently large separations between walls, they agree with results obtained in the bulk [8].

In the following sections, a description of the model is made and comparisons with results obtained elsewhere are given. Calculations of the slip velocity and the birefringence for different Coulombic bead repulsions are also described.

The model

The model of the elastic dumbbell includes a nonlinear Warner spring [5] and electrostatic repulsion between beads, each with an effective charge. The dumbbell concentration is low and dumbbell–dumbbell interactions are neglected. Coulombic repulsion is modeled as point charges of magnitude q separated by the end-to-end distance of the dumbbell (r'). As in Ref. [8], the charge q assigned to the beads is an effective value intended to simulate the charge repulsion between ionized sites that are distributed along the backbone of the real polyelectrolyte. A Coulombic force law characterized by a dielectric constant ε which is independent of the concentration of the counterions in the solvent is assumed.

The solution flows between narrow channels under shear flow with a velocity gradient of magnitude $\dot{\gamma}'$. The shear flow is generated by moving two parallel walls along the x-axis in opposite directions with velocity $v_x = \dot{\gamma}' y'_c$.

The channel walls are considered to be either neutral or repulsive. In the latter case, an average force is assumed to interact between the charged walls and the dumbbell's center of mass and is given by the potential [9]

$$v(y'_c) = K_w k_B T \left\{ \exp\left[-\lambda \left(\frac{y'_c + H}{\sigma} \right) \right] + \exp\left[-\lambda \left(\frac{H - y'_c}{\sigma} \right) \right] \right\} . \quad (1)$$

This expression accounts for the interaction potential existing between the charged walls, separated by a distance $2H$, and the dumbbell represented by a charged sphere of diameter σ. λ is the Debye inverse nondimensional screening length and $k_B T$ is the Boltzmann temperature. K_w is an intensity parameter which depends on the solvent, the effective charge and the size of the dumbbell, and finally, y'_c stands for the distance from the center of the channel to the dumbbell center of mass $(-H \le y'_c \le H)$.

To derive the equations of motion for the dumbbell, the force balance for each dumbbell is expressed with respect to the internal coordinates (x', y', z') and the center-of-mass coordinates (x'_c, y'_c, z'_c):

$$-\frac{\zeta r'}{\sqrt{Na}}(\mathbf{r}' - \dot{\gamma}'\Gamma \cdot \mathbf{r}') - 2k_B T\nabla' \ln(\psi) - \frac{6Nk_B T}{R^2}\left(\frac{\mathbf{r}'}{1-\left(\frac{\mathbf{r}'}{R}\right)^2}\right) + \frac{2q^2\mathbf{r}'}{\epsilon r'^3} = 0 \quad (2)$$

$$-\frac{\zeta r'}{\sqrt{Na}}\left(\mathbf{r}'_c - \dot{\gamma}'\,\Gamma \cdot \mathbf{r}'_c\right) - \frac{k_B T}{2}\nabla'_c \ln(\psi) + \frac{\lambda K_w}{\sigma}\left\{\exp\left[-\lambda\left(\frac{y'_c + H}{\sigma}\right)\right] - \exp\left[-\lambda\left(\frac{H - y'_c}{\sigma}\right)\right]\right\}\mathbf{j} = 0 \ , \quad (3)$$

where r' is the end-to-end vector, $R = Na$ is the maximum length of the dumbbell, N is the number of subunits of length a in the chain, ζ is the Stoke's law friction coefficient for the dumbbell in equilibrium and Γ is the transpose of the velocity gradient tensor. In Eq. (3) $\mathbf{j}$ is a unit vector perpendicular to the walls and the gradient ∇'_c refers to the dumbbell center-of-mass coordinates.

The first term in Eqs. (2) and (3) represents the frictional interaction between the solvent and the dumbbell and the second term is the Brownian contribution to the dumbbell motion, where ψ is the configurational probability density function. In Eq. (2) the interaction between beads is represented by the nonlinear elastic spring (third term) and the effects of the electrostatic repulsion are included in the fourth term of this equation.

As a first approximation, the interactions between the charged walls and the dumbbell are represented by those existing between a charged sphere of average diameter σ (located at a distance y'_c from the center of the channel) and the walls. This contribution is given by the third term in Eq. (3).

The velocity gradient tensor is given by the matrix

$$\Gamma = \begin{pmatrix} 0 & 1 & 0 \\ 0 & 0 & 0 \\ 0 & 0 & 0 \end{pmatrix} \ . \quad (4)$$

To obtain the rate of change of the end-to-end vector we combine Eqs. (2) and (3) with the continuity equation:

$$\frac{\partial\psi}{\partial t'} = -\nabla'_c \cdot \left(\mathbf{r}'_c\psi\right) - \nabla' \cdot \left(\mathbf{r}'\psi\right) \ . \quad (5)$$

It is assumed that ψ depends on the internal coordinates $\mathbf{r}'$ and the center-of-mass coordinates y'_c.

These equations may be expressed in terms of the dimensionless variables $r = \frac{r'}{R}, t = \frac{t'}{\theta}$ and $\dot{\gamma} = \dot{\gamma}'\,\theta$, where θ is the Zimm relaxation time $\zeta R^2/(6Nk_B T)$. The distance from the center of mass to the symmetry line of the channel and the size of the dumbbell are rescaled with $y_c = y'_c/H$ and $\epsilon = \sigma/(H)$.

Substituting Eqs. (2) and (3) into Eq. (5), multiplying the resulting equation by $\mathbf{rr}$ and then integrating over the configuration space, (assuming that ψ goes to zero at the limits of integration) we obtain the equation for the second moments of the distribution function $\langle\mathbf{rr}\rangle$.

$$\begin{aligned}\frac{\mathrm{d}}{\mathrm{d}t}\langle\mathbf{rr}\rangle = \dot{\gamma}\langle y^2\mathbf{ij} + y^2\mathbf{ji} + 2xy\mathbf{ii}\rangle \\ - \frac{2}{\sqrt{N}}\frac{1}{r}\left(\frac{1}{1-r^2} - \frac{E}{3Nr^3} + \frac{1}{3Nr^2}\right)\langle\mathbf{rr}\rangle \\ + \frac{2}{3N^{\frac{3}{2}}}\frac{1}{r}\mathbf{I} + \frac{\sqrt{N}}{12r}\epsilon^2\frac{\mathrm{d}^2}{\mathrm{d}y_c^2}\langle\mathbf{rr}\rangle \\ + \frac{\lambda K_w\sqrt{N}}{6r}\left\{\exp\left[-\lambda\left(\frac{y_c+1}{\epsilon}\right)\right] - \exp\left[-\lambda\left(\frac{1-y_c}{\epsilon}\right)\right]\right\} \\ \times\left(\lambda\langle\mathbf{rr}\rangle - \epsilon\frac{\mathrm{d}}{\mathrm{d}y_c}\langle\mathbf{rr}\rangle\right) \ , \end{aligned} \quad (6)$$

where $\mathbf{i}$ and $\mathbf{j}$ are unit vectors in the flow direction and perpendicular to the flow, respectively. $\mathbf{I}$ is the unit tensor and E is the dimensionless charge density parameter $E = q^2/\left(ek'_B TR\right)$ viewed as the ratio of electrostatic to thermal energy. This equation is a generalization of the one obtained by Dunlap and Leal [8] when the system is in the bulk and interactions with the walls are ignored.

From Eq. (6) we obtain the corresponding equations for each component of the tensor $\langle\mathbf{rr}\rangle$ in stationary conditions:

$$A\frac{\mathrm{d}^2}{\mathrm{d}y_c^2}\langle x^2\rangle + B\langle x^2\rangle + C\langle xy\rangle + D + Gz\langle x^2\rangle - G\epsilon\frac{\mathrm{d}}{\mathrm{d}y_c}\langle x^2\rangle = 0 \quad (7)$$

$$\begin{aligned} A\frac{\mathrm{d}^2}{\mathrm{d}y_c^2}\langle xy\rangle + B\langle xy\rangle + \frac{C}{2}\langle y^2\rangle + Gz\langle xy\rangle - G\epsilon\frac{\mathrm{d}}{\mathrm{d}y_c}\langle xy\rangle = 0 \\ A\frac{\mathrm{d}^2}{\mathrm{d}y_c^2}\langle y^2\rangle + B\langle y^2\rangle + D + Gz\langle y^2\rangle - G\epsilon\frac{\mathrm{d}}{\mathrm{d}y_c}\langle y^2\rangle = 0 \\ A\frac{\mathrm{d}^2}{\mathrm{d}y_c^2}\langle z^2\rangle + B\langle z^2\rangle + D + Gz\langle z^2\rangle - G\epsilon\frac{\mathrm{d}}{\mathrm{d}y_c}\langle z^2\rangle = 0 \ , \end{aligned} \quad (8)$$

where the parameters A, B, C, D and G are given as follows

$$A = \frac{\sqrt{N}\epsilon^2}{12r}, \quad B = -\frac{2}{\sqrt{N}}\frac{1}{r}\left(\frac{1}{1-r^2} - \frac{E}{3Nr^3} + \frac{1}{3Nr^2}\right) \ ,$$

$$C = 2\dot{\gamma}, \quad D = \frac{2}{3N^{\frac{3}{2}}}\frac{1}{r},$$
$$G = \frac{\lambda K_w \sqrt{N}}{6r}\left\{\exp\left[-\lambda\left(\frac{y_c+1}{\epsilon}\right)\right] - \exp\left[-\lambda\left(\frac{1-y_c}{\epsilon}\right)\right]\right\} \quad (9)$$

Numerical solutions are obtained for these equations. However, when neutral walls are considered, exact solutions can be obtained and are given by

$$\begin{aligned}
\langle y^2\rangle &= c_1\cosh(\alpha y_c) + \frac{D}{A\alpha^2} \\
\langle xy\rangle &= c_{1_p}\cosh(\alpha y_c) + A_1 + A_2 y_c \sinh(\alpha y_c) \\
\langle x^2\rangle &= c_{1_{pp}}\cosh(\alpha y_c) + c_0 + c_2 y_c \sinh(\alpha y_c) \\
&\quad + c_3 y_c^2 \cosh(\alpha y_c) \ ,
\end{aligned} \quad (10)$$

where the constants are defined as follows:

$$\begin{aligned}
&\alpha^2 = -\frac{B}{A}, \quad c_1 = \frac{D}{A\alpha^2\cosh(\alpha)}, \quad A_1 = \frac{CD}{2A^2\alpha^2}, \\
&A_2 = \frac{Cc_1}{4A\alpha} \quad c_0 = \left(\frac{c}{A}A_1 + \frac{D}{A}\right)/\alpha^2, \\
&c_2 = -\left(\frac{C}{A}c_1 + 2c_3\right)/\alpha, \quad c_3 = \frac{CA_2}{2A\alpha} \\
&c_{1p} = -\frac{A_1}{\cosh(\alpha)} + 2A_2\tanh(\alpha), \\
&c_{1_{pp}} = \frac{(M-c_0)}{\cosh(\alpha)} - 2c_2\tanh(\alpha) - 2c_3 \ .
\end{aligned} \quad (11)$$

Here M is the value of the moment $\langle x^2\rangle$ at the wall ($y_c = \pm 1$). In Eq. (9) we have assumed that the moments $\langle y^2\rangle$ and $\langle xy\rangle$ are zero at the walls and that the first derivatives of all the moments are zero on the centerline of the channel. A similar approach has been used by Goh et al. [1].

The rheological properties for steady-shear flow are calculated in standard form from the added stress σ due to n dumbbells per unit volume:

$$\sigma = n\langle \mathbf{F}_{\text{connector}}\mathbf{r}'\rangle \ , \quad (12)$$

where $\mathbf{F}_{\text{connector}}$ is the effective force between beads including the Coulombic repulsion. After substitution and using the preaveraging approximation in nondimensional form, Eq. (11) becomes

$$\frac{\sigma}{3nkT} = N\left[\frac{1}{1-r^2} - \frac{E}{3Nr^3}\right]\langle \mathbf{rr}\rangle \ . \quad (13)$$

The steady-shear viscosity is obtained by calculating the ratio of shear stress σ and shear rate $\dot{\gamma}$.

Results

To compare the result of this model with those of similar approaches, viscosity profiles across the channel calculated from Eq. (12) for $N = 1, \frac{1}{2} \le \frac{1}{\epsilon} \le 5$ and for a low shear rate ($\dot{\gamma} = 0.1$) are given in Fig. 1. In this case, Coulombic interactions between beads ($E = 0$) and interactions with the walls are not taken into account. Comparison with results obtained by Brunn and Grisafi [2] shows that agreement is obtained for relatively large values of the parameter $\frac{1}{\epsilon}$ (i.e. when the wall separation is not too small). The dimensionless viscosity represents the viscosity relative to that of a very wide channel ($\frac{1}{\epsilon} = 100$). Notice that as the wall separation increases, the viscosity tends to a constant value except in the region adjacent to the wall.

For arbitrary values of the shear rate, viscosity profiles are shear-rate dependent and thus they depart from those of the linear dumbbell used by Brunn and Grisafi. Again, for $N = 1$, $E = 0$ and two different shear rates, Fig. 2 shows the normalized viscosity as a function of channel width. Values similar to those of Grisafi and Brunn [3] are obtained for separations $\frac{1}{\epsilon} \ge 10$. For values $\frac{1}{\epsilon} < 10$, the viscosities obtained are larger than predicted.

The behavior of the average viscosity for different shear rates is shown in Fig. 3. It can be seen that as the channel widens, the average viscosity tends to that of the bulk obtained by Dunlap and Leal. In Fig. 3a, predictions for a relatively flexible dumbbell (low repulsion) with neutral and repulsive walls are shown. The bulk viscosity shear-thickens and describes a maximum at $\dot{\gamma} = 10$ after which a region of shear thinning is apparent. In the case of neutral walls, as the wall separation is reduced, the viscosity lowers, but the curves follow the same trend with a pronounced shear-thickening region. For charged walls, qualitatively the same effect is manifested, but viscosity values are even

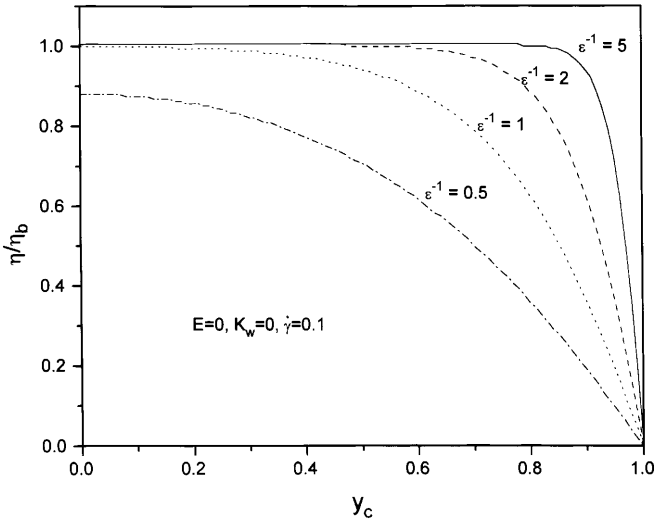

Fig. 1 Viscosity profiles relative to a wide channel ($\epsilon^{-1} = 100$) calculated for $N = 1$ and different wall separations (ϵ^{-1}). Coulombic repulsion is not included ($E = 0$) and neutral walls are considered ($K_w = 0$)

smaller than those with neutral walls. On the other hand, results are nearly independent of the size of the channel and the charge of the walls when the shear rate is about 1000.

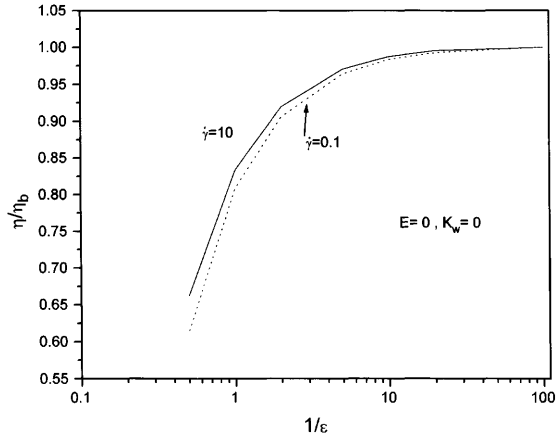

Fig. 2 Average viscosity for two different shear rates, obtained for different wall separations for the case $N = 1, E = 0$ and $K_w = 0$

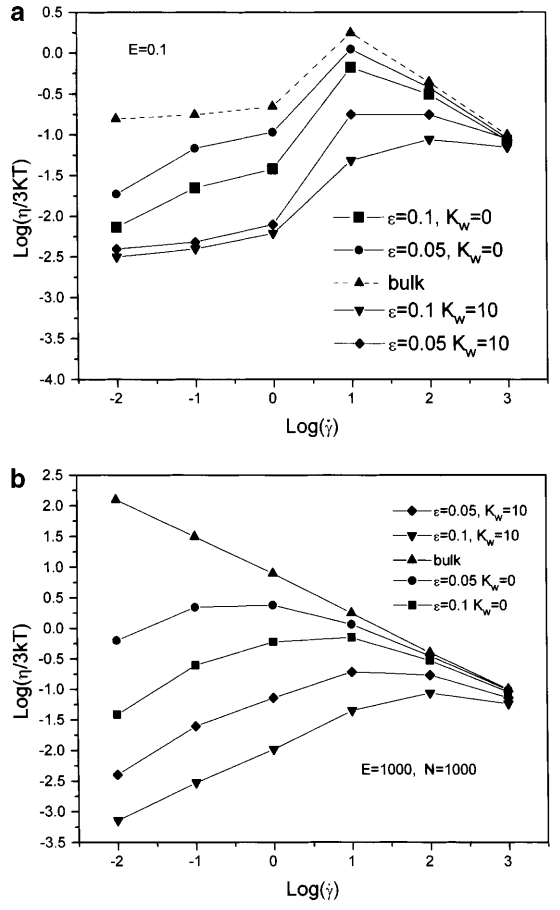

Fig. 3a, b Average viscosity for different shear rates including charged and uncharged walls for $N = 1000$. **a** $E = 0.1$ and **b** $E = 1000$

In the case of high repulsion ($E = 1000$), where the dumbbell conformation is similar to that of a rigid rod, Fig. 3b shows a variation in the average viscosity with shear rate for different wall separations with and without charge on the walls. In the bulk, continuous shear thinning of the viscosity with a nearly constant slope (-0.624) is observed. As the wall separation is reduced, the viscosity at small shear rates is lower than that of the bulk and so a maximum is apparent at intermediate shear rates. The maximum shifts to higher shear rates for smaller wall separations and the effect of the charge on the wall for a given separation is to decrease the viscosity even further. Again, for very high shear rates both the effects of wall repulsion and wall separation tend to disappear.

In Fig. 4 viscosity profiles across the channel are plotted for various shear rates at fixed channel width. Predictions of viscosity for a flexible and rigid conformation with and without wall repulsion are shown. The overall effect of the charge on the walls is to decrease the viscosity in the regions adjacent to the rigid boundaries,

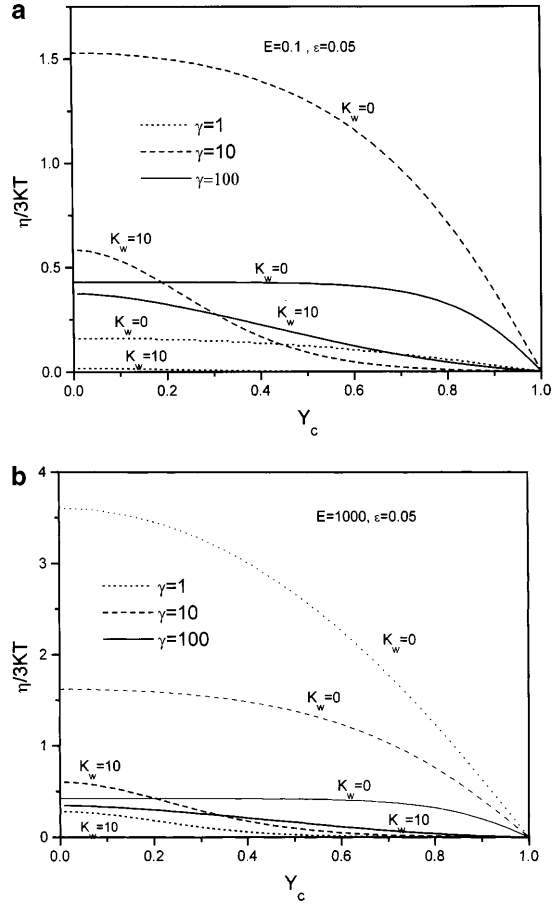

Fig. 4a, b Viscosity profiles for different shear rates, wall repulsions and for a fixed wall separation. **a** $E = 0.1, K_w = 0$ and $K_w = 10$; **b** $E = 1000, K_w = 0$ and $K_w = 10$

and also to induce a steeper drop in the viscosity across the channel. Notice the pronounced shear-thickening effect in flexible dumbbells for both charged and noncharged walls. In contrast, in Fig. 4b, rigid dumbbell profiles show a purely shear-thinning behavior, corresponding to that shown in Fig. 3b for $\varepsilon = 0.05$ and $K_w = 0$.

The effect of increasing the wall-repulsion potential on the average viscosity is depicted in Fig. 5 for a fixed shear rate and moderate bead repulsion. A strong dependence of wall repulsion on the viscosity is observed, and for highly repulsive walls the viscosity is very small in the whole channel.

As predicted previously, a consequence of increasing confinement is that the average viscosity becomes dependent on the characteristic length of the geometry considered. In a number of analyses this phenomenon is characterized by a slip velocity, which can be evaluated using the following relation [1]

$$U_s = \frac{1}{\eta_s}\int_0^1 dy(\sigma_{xy}^{\infty} - \sigma_{xy}) \ , \tag{14}$$

where σ_{xy}^{∞} is the shear stress due to the contribution of the macromolecules in the center of the channel and η_s is the solvent viscosity.

The behavior of the slip velocity as a function of the shear rate calculated using Eq. (14) is shown in Fig. 6 for $E = 0.1$ and $E = 1000$ for different wall separations. The behavior of the slip velocity is illustrated for charged and uncharged walls as well.

In Fig. 6a, for a flexible dumbbell, the slip velocity is a growing function of the shear rate and attains an upper limit at the highest shear rates. For neutral walls, the slip velocity is slightly larger than that with charged walls in the low-shear-rate interval. In the presence of a charged wall, the opposite behavior is observed in the high-shear-rate region.

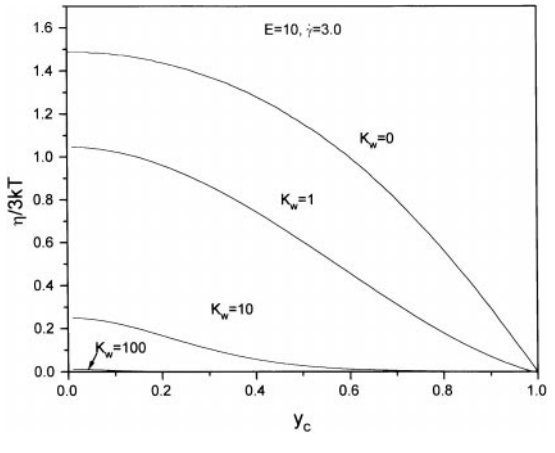

Fig. 5 Local viscosity in a channel with $\epsilon = 0.05$ for different wall repulsions, and for a fixed shear rate and bead–bead repulsion

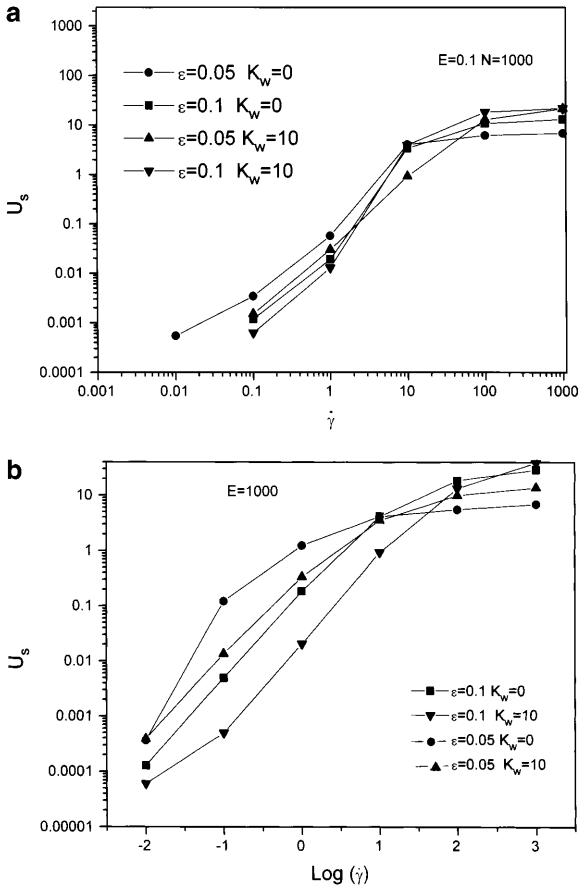

Fig. 6a, b Slip velocity for different shear rates and wall separations for charged and neutral walls ($N = 1000$, **a** $E = 0.1$ and **b** $E = 1000$

Similar results were obtained by Goh et al. [1] for a narrower channel ($\epsilon = 0.77$) using a Warner molecule with neutral walls; however, the slip velocity values are smaller than those presented here probably due to differences in the models.

In Fig. 6b we compare the results for two wall separations. In this case the molecule is almost totally extended and the slip velocity values are larger than those for lower bead interaction ($E = 0.1$). The slip velocity is a growing function of the shear rate in all cases and is greater for the narrower channels. The slip velocity is comparatively greater for uncharged walls at low shear rates but becomes lower at higher shear rates.

As is well known, the method of Mooney may be used to evaluate the slip velocity by comparing flow curves generated in a specific geometry as the confinement is increased. Plots were obtained for $E = 0.1$ and $E = 1000$ for uncharged walls. According to the Mooney method [10], for a fixed macroscopic wall shear stress (τ_w), if the apparent wall shear rate ($\dot{\gamma}_w$) from different flow curves is a linear function of the inverse wall

separation, then it is possible to evaluate the slip velocity using the following relationship [11]

$$U_s = \frac{\partial(\dot{\gamma}_w)}{4\partial(1/H)}, \quad \tau_w \text{ constant} , \tag{15}$$

where $2H$ is the wall separation.

The nondimensional shear rate is plotted for the inverse wall separation (4ϵ) for three different shear-stress values in Fig. 7a. The results show a very good linear correlation ($R \geq 0.999$) for the whole range of wall separations considered. The slip velocity is greater for the case when the chains are more extended ($E = 1000$) than for the case when the repulsive Coulombic interactions are negligible ($E = 0.1$) (Fig. 7b). This result is in agreement with experimental results of slip velocity for rigid (or semirigid) and flexible macromolecules [12]. The Mooney method has also been applied to other systems, such as charged colloidal particles flowing in narrow repulsive channels [13], where it is possible to evaluate the slip velocity from the linear plot of shear rate versus inverse characteristic length.

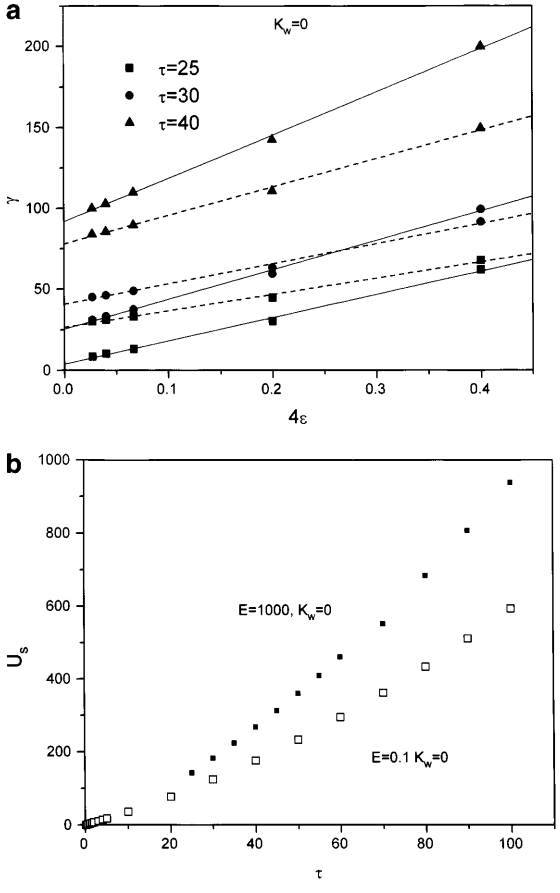

Fig. 7 a Mooney plots for dilute polyelectrolyte solutions simulated with $N = 1000$ and neutral walls for different shear stresses. $E = 0.1$ (- - -), $E = 1000$ (—) **b** slip velocity as a function of shear stress for flexible (□) and rigid (■) molecules

Finally, flow-birefringence calculations were carried out in a wide channel ($\epsilon = 0.01$) for three different bead Coulombic repulsions ($E = 0.1, 100$ and 1000)

Birefringence is determined using the following relationship:

$$\frac{\Delta n}{ncB} = \left[\left(\langle x^2\rangle - \langle y^2\rangle\right)^2 + 4\langle xy\rangle^2\right]^{\frac{1}{2}} , \tag{16}$$

where Δn is the birefringence, n is the refractive index, c is the polymer concentration and B is a constant which depends on the molecule polarizabilities, molecular weight and refractive index.

The birefringence has been measured in bulk flow without the influence of walls [7]; however, as shown in Fig. 8, the birefringence measured in the channel center as a function of the shear rate for different wall separations depicts an interesting behavior for the three Coulombic repulsion levels. Evidently, the effect of confinement is to reduce the magnitude of the birefringence especially over the range of low shear rates. For very slow flows, and in the case of an extended rigid conformation, confinement reduces the birefringence to levels seen in flexible molecules. Notice that as E is increased, the shape of the birefringence curve changes from an S shape (observed in flexible molecules) to a concave shape characteristic of a rigid molecule. The reduction in birefringence as the wall separation decreases is a very interesting behavior which is caused by the decrease in the magnitude of the moment $\langle x^2\rangle$ as the confinement increases, with no appreciable change in $\langle y^2\rangle$ and $\langle xy\rangle$. This suggests that the low birefringence levels are due to the increase in the $\langle z^2\rangle$ moment, implying that the dumbbells are oriented along the vorticity direction.

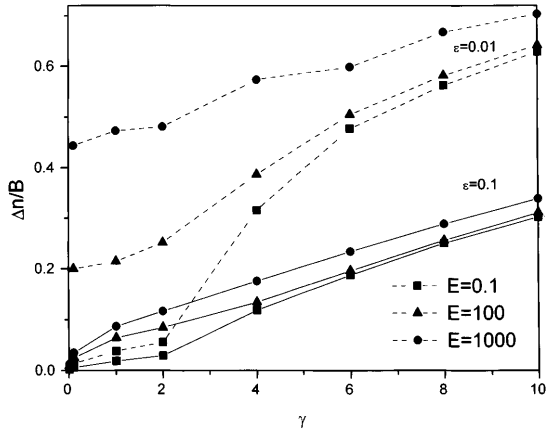

Fig. 8 Birefringence calculations for dilute polyelectrolyte solutions in the center of the channel for $N = 1000$, for $\epsilon^{-1} = 100$ and $\epsilon^{-1} = 10$ and different Coulombic bead repulsions

Discussion

The flow of polymer solutions in confined geometries is largely influenced by wall effects, which become important when the macromolecular size is comparable to the dimensions of the flow domain. In simple shear, it is found that the concentration of macromolecules decreases towards the walls, resulting in a reduction in the viscosity in the wall region. Close to the wall, the viscosity decreases because the wall layer is depleted of molecules and also due to the fact that molecules are oriented parallel to the wall and thus they do not contribute to the shear stress. As observed in Figs. 1 and 2, the wall layer or slip layer increases in size as the wall separation decreases. These results are also in agreement with those of Biller and Petruccione [14].

In Fig. 3 the change in E from 0.1 to 1000 evidences the increase in the zero-shear-rate viscosity due to increased coil expansion. For large E, the solution is shear-thinning in the bulk, reflecting the transition towards an extended, rigid rod. The slope of the viscosity–shear-rate curve in this case is close to $-2/3$, which corresponds to the value of the rotation period of a rod in unbounded shear flow at high shear rates [15]. On the other hand, the shear-thickening behavior in the viscosity is a consequence of the increase in bead friction with increasing dumbbell extension. An intersecting point to mention is that the maximum in the viscosity with shear rate is also found as the channel shortens. In Fig. 3b, the shear-thickening region widens and the maximum is shifted to higher shear rates as the channel narrows. This effect is more pronounced with charged walls, indicating that confinement induces enhanced hydrodynamic friction.

The reduction of the viscosity near the wall is less sensitive to the imposed shear rate than that in the middle of the channel. In fact, curves with different shear rates converge near to the wall, but the effect of the shear rate is lower when the walls are charged (Fig. 4). The results shown in Fig. 4 also illustrate that the state of the wall has a very important effect upon the depletion – layer thickness. Comparison of the slip layer for neutral walls with that for charged walls (Fig. 4) shows that the size of the slip layer is larger at low shear rates, especially when the dumbbell adopts an extended and rigid conformation. It has been predicted [16] that the mean depletion layer in rigid molecules decreases as the shear rate increases form equilibrium to moderate values. These results are explained by the fact that at moderate shear rates, a dumbbell tends to align itself with the direction of the flow, and thus its center of mass can approach the wall more closely than in the flow at very low shear rates. An increase in the size of the depletion layer may be expected at very high shear rates [16]

With respect to results shown in Fig. 7b, it is apparent that decreasing the flexibility of the dumbbell induces a greater slip velocity for a given shear stress. Nonequilibrium molecular dynamics simulations of chains sheared between two atomic walls [17] agree with these results. Stiffer chains align more with the fluid than the flexible ones to reduce the flow resistance.

Velocity profiles in simple shear flow of polymeric liquids are usually linear, but in some cases large slip is observed near the walls. Slip has been predicted by molecular dynamics simulations of short chains [18, 19]. As a result of this large slip, the actual shear rate is much lower than the nominal shear rate. If the viscosity is calculated using the nominal shear rate, the resulting mean viscosity decreases as the wall separation decreases, as observed in Fig. 3. The actual shear rate in the channel, however, is significantly different from the nominal shear rate [20]. If the viscosity is determined using the actual shear rate, then the mean viscosity of the fluid should increase as the wall separation diminishes, and the increase should be larger as the wall separation becomes comparable with the dumbbell dimensions. In fact, experiments in confined channels with noncharged molecules between neutral walls have shown that as the thickness of the fluid region decreases below $6\sigma(\epsilon \geq 0.167)$, the viscosity of the fluid increases dramatically [21, 22]. Nevertheless, it is possible to estimate the actual shear rate from the curves in Fig. 7a from the intercept as $\epsilon \to 0$. This extrapolation corresponds to the actual shear rate obtained in very wide channels (bulk flow), where the slip effects are negligible for a given shear stress. Consequently, the estimated shear rate would be lower than the nominal shear rate, and the resulting viscosities in turn would be higher than those shown in the curves in Fig. 3.

Another important issue of the present results is the comparison of the slip velocities calculated from Eq. (14) on one hand, and from Eq. (15) on the other hand. The definition of the slip velocity by Brunn [23] considers the difference between the shear stress near the wall and the shear stress in the channel center. This definition holds irrespective of the size of the flow geometry. The Mooney method, on the other hand, considers different wall separations. As the separation becomes smaller, the effect of the slip layer increases progressively for a given shear stress. In turn, the average viscosity measured in flow regions with decreasing separation of the walls diminishes progressively. However, Brunn [23] has also considered this case and defines the slip coefficient to be proportional to the slope of the curve of the fluidity versus the inverse length of the geometry. The data included in Fig. 7a give the shear rate as a function of the inverse length at constant stress. These data can be readily transformed into plots of fluidity versus inverse length by dividing the shear rate by the constant shear stress. Indeed, Brunn obtains

a linear relation of fluidity versus inverse length, in agreement with the results in Fig. 7. Figure 7b illustrates the variation in the slope of the shear rate–inverse-length curve with shear stress. The shape of the resulting curve is in agreement with the results of Khare et al. [20] for the prediction of the slip velocity using a bead–spring model. Similarly, the results shown in Fig. 6 are in agreement with those of Goh et al. [1], in that the nonlinear dumbbell model predicts that the slip velocity in Eq. (14) tends to a limiting value for increasing shear rate. As already mentioned, the results presented in Fig. 7b are in qualitative agreement with experiment.

Conclusions

In this work, the rheological behavior of dilute polyelectrolyte solutions in a confined planar geometry has been studied. Using a dumbbell model with a nonlinear Warner spring force for polymers in solution under shear flow, it is possible to reproduce the behavior in the bulk when the channels are about 100 times larger than the size of the polymers. An interesting behavior is obtained for narrower channels, i.e. a viscosity dependent on the size of the channel, on the electrical repulsion between the beads of the molecular chains and on the wall-repulsion potential.

The slip velocity is also dependent on the size of the channels and on the bead repulsion. The calculated velocity is a growing function of the shear rate as observed by other authors. For high shear rates, the slip velocity is greater for repulsive walls than for neutral walls; probably due to the migration of molecules through the center of the channel and to the orientational effects induced by the flow. Our consideration of the Mooney method seems to be plausible in the sense that the behavior of the calculated slip velocity is similar to the experimental one reported by several authors.

Acknowledgements M.A. Valdez acknowledges support from the Consejo Nacional de Ciencia y Tecnología and from the Universidad de Sonora and the Instituto de Investigación en Materiales.

References

1. Goh CJ, Atkinson JD, Pan-Thien N (1985) J Chem Phys 82: 988
2. Brunn PO, Grisafi SJ (1987) J Non-Newtonian Fluid Mech 24: 343– 363
3. Grisafi SJ, Brunn PO (1989) J Rheol 33: 47–67
4. Valdez MA, Tejero J (1994) Rheol Acta 33: 125–135
5. Fuller GG, Leal LG (1981) J Non-Newtonian Fluid Mech 8: 271–310
6. de Gennes PG (1979) Scaling concepts in polymer physics. Cornell University Press, Ithaca
7. Dunlap PN, Wang CH, Leal LG (1987) J Polymer Sci Part B Polym Phys 25: 2211–2238
8. Dunlap PN, Leal LG (1984) Rheol Acta 23: 238–249
9. González-Mozuelos P, Alejandre J, Medina-Noyola M (1991) J Chem Phys 95: 8337
10. Mooney M (1931) J Rheol 2: 210
11. Harris J (1977) Rheology and non-Newtonian flow. Longman, London
12. de Vargas L, Manero O (1989) Polym Eng Sci 29: 1332
13. Valdez MA, Manero O (1997) J Colloid Interface Sci 190: 81–91
14. Biller P, Petruccione F (1987) J Non-Newtonian Fluid Mech 25: 347–36
15. Ötinger HC (1988) J Rheol 32: 135
16. de Pablo JJ, Öttinger HC, Rabin Y (1992) AIChE J 38: 273–283
17. Peters GH, Tildesley DJ (1996) Phys Rev E 54: 5493
18. Thompson PA, Robbins MO, Grest GS (1995) Isr J Chem 35: 93
19. Manias E, Hadziioannou G, Bitsanis I, Ten Brinke G (1993) Europhys Lett 24: 99
20. Khare R, de Pablo JJ, Yethiraj A (1996) Macromolecules 29: 7910–7918
21. Granick S (1991) Science 253: 1374
22. Luengo G, Schmidtt FJ, Hill R, Israelachvili J (1997) Macromolecules 30: 2482
23. Brunn PO (1976) Rheol Acta 15: 23–29